Article

New 5-aryl-1H-imidazoles display in vitro antitumor activity against apoptosis-resistant cancer models, including melanomas, through mitochondrial targeting

Véronique Mathieu, Emilie Van Den Berge, Justine Ceusters, Tomasz Konopka, Antonin Cops, Céline Bruyère, Christine Pirker, Walter Berger, Tran trieu-Van, Didier Serteyn, Robert Kiss, and Raphael Robiette

Just Accepted

New 5-aryl-1*H*-imidazoles display *in vitro* antitumor activity against apoptosis-resistant cancer models, including melanomas, through mitochondrial targeting

Véronique Mathieu,[*,†] *Emilie Van Den Berge,*[‡] *Justine Ceusters,*[§] *Tomasz Konopka,*[#] *Antonin Cops*[†], *Céline Bruyère*[†], *Christine Pirker,*[¶] *Walter Berger,*[&] *Tran Trieu-Van,*[‡] *Didier Serteyn,*[§] *Robert Kiss*[†] *and Raphaël Robiette*[*,‡]

[†]Laboratoire de Toxicologie, Faculté de Pharmacie, Université Libre de Bruxelles (ULB), Boulevard du Triomphe, CP205/1, B-1050 Brussels, Belgium.

[‡]Institute of Condensed Matter and Nanosciences, Université catholique de Louvain, Place Louis Pasteur 1 box L4.01.02, B-1348 Louvain-la-Neuve, Belgium.

[§] Center for Oxygen, Research and Development, Institute of Chemistry B6a, University of Liège, Sart Tilman, 4000 Liège, Belgium.

[#] BioSystems, BioModeling and BioProcesses Group, Université Libre de Bruxelles, CP165/61, B-1050 Brussels, Belgium.

[¶] Department of Thoracic Surgery, Medical University Vienna, Vienna, Austria.

[&] Department of Medicine I, Institute of Cancer Research, Medical University Vienna, Vienna, Austria.

RECEIVED DATE

AUTHOR INFORMATION

* Phone: +32-2-6505179. E-mail: vemathie@ulb.ac.be (V.M.; biology). Phone: +32-10-479176. Fax: +32-10-474168. E-mail: raphael.robiette@uclouvain.be (R.R.; chemistry).

ABSTRACT

We designed and synthesized 48 aryl-1*H*-imidazole derivatives and investigated their *in vitro* growth inhibitory activity in cancer cell lines known to present various levels of resistance to pro-apoptotic stimuli. The IC_{50} *in vitro* growth inhibitory concentration of these compounds ranged from >100µM to single digit µM. Among the most active compounds, **2i** displayed similar *in vitro* growth inhibition in cancer cells independently of the cells' levels of resistance to pro-apoptotic stimuli, and was found to be cytostatic in melanoma cell lines. Compound **2i** was then tested by the National Cancer Institute Human Tumor Cell Line Anti-Cancer Drug Screen, and the NCI COMPARE algorithm did not reveal any correlation between its growth inhibition profiles with the NCI database compound profiles. The use of transcriptomically characterized melanoma models then enabled us to highlight mitochondrial targeting by **2i**. This hypothesis was further confirmed by reactive oxygen production measurement and oxygen consumption analysis.

INTRODUCTION

Since the beginning of anticancer chemotherapy in the 1950s, the survival rate associated with several cancer types has been markedly improved, e.g. testicular cancers or several types of leukemia and lymphoma that can even be cured.[1, 2] In contrast, despite the enrichment of the chemical libraries used in oncology for over half a century with natural as well as synthetic compounds, other cancer types remain associated with a dismal prognosis due to their acquired (e.g. multidrug resistance phenotype)[3, 4] or innate (intrinsic apoptosis resistance) [5, 6] resistance to chemotherapeutic insults. Most of the compounds used to treat cancer patients are cytotoxic and pro-apoptotic agents.[7] Cancers associated with dismal prognoses, include, but are not limited to, glioma,[8] advanced melanoma,[9, 10] non-small cell lung carcinoma,[11] head and neck carcinoma,[12] esophageal carcinoma[13] and pancreatic carcinoma.[14]

Aryl-1H-imidazoles are key chemical structures that display a wide range of biological and pharmacological activities.[15-17] Biologically active aryl-1H-imidazoles include compounds with potent *in vitro* antifungal activity, inhibitors of β-glucosidase, molecules with anti-inflammatory properties, substances exhibiting activin receptor-like kinase 5 (ALK5) inhibitory activity, antagonists of NPY5 receptors, potent Na^+ channel blockers and molecules with antitubulin and antiproliferative activities against cancer cells.[15-17] In a previous report, we demonstrated that 5-aryl-1H-imidazoles embedded in a macrocycle via a connection at the C2 and ortho-aryl positions (**1**) display interesting binding activities toward biological targets that are important actors in the central nervous system such as the A_3 adenosine (*h*) receptor, dopamine D_1 (*h*) receptor and chlorine channel (GABA-gated).[18]

Here, we report on (i) the identification and optimization of 5-aryl-1H-imidazoles as potential anticancer agents, (ii) the characterization of the *in vitro* cytostatic versus cytotoxic anti-cancer activity of these compounds, and (iii) the partial deciphering of their mechanism of action in melanoma cells. The revealed mechanism led us to highlight the targeting by this type of compound of mitochondrial metabolism, which is known to be reprogrammed in cancer cells.[19] The original mechanism of action we

identified for the most active compounds under study opens chemistry to several new anti-cancer avenues.

CHEMISTRY

The synthesis of all studied 2-alkoxy-5-aryl-*1H*-imidazole derivatives starts from intermediate **5,** which was prepared using a highly regioselective methodology previously developed in our lab (Scheme 1).[20] The strategy for forming the macrocycle is based on three key steps: a nucleophilic aromatic substitution, a Suzuki coupling and a ring closure metathesis reaction.[18] The nucleophilic aromatic substitution places the first arm on the scaffold (R[1]), while the Suzuki coupling allows the second alkene chain (R[2]) to be introduced. Some boronic acids used in this latter step were synthesized from corresponding bromo derivatives (see the SI). Finally, the two last steps are the ring closure metathesis, using the second-generation Grubbs catalyst, and the hydrogenation of the resulting double bond. This strategy allowed us to obtain a series of macrocycles (**1a-j**), as well as intermediates, during the synthesis (**2a-aa**, **4a**) (Table 1). We also synthesized imidazoles missing the alkene chain on C(2) of the imidazole (**6**) or the aryl group (**14**) as well as an imidazole bearing the aryl group in 4 position (**15**) to investigate the influence of these structural motifs on the *in vitro* growth inhibition activity of various cancer cell lines.

It is important to mention that a detailed NMR and HPLC study revealed that some of our macrocycles (**1**) are chiral.[21] Indeed, due to their cyclophane-type structure, macrocycles **1a-f** are planar chiral molecules. In contrast, their superior analogues **1h-j** isomerize rapidly at room temperature. Given the importance of chirality for biological activities, we separated the two enantiomers of **1a** to separately test their *in vitro* growth inhibition activity in cancer cells.

We decided to also synthesize the corresponding 2-amidoimidazoles to investigate the influence of the electronic properties of the imidazole ring on *in vitro* cancer cell growth inhibition. We first planned to

prepare these derivatives by applying the same methodology as the synthesis of the 2-alkoxy-imidazole derivatives (**1**). However, our attempts to achieve the nucleophilic aromatic substitution of the sulfone group by an amine were unsuccessful. Thus, we turned our efforts to the implementation of the methodology developed by the E. Van der Eycken group.[22, 23] This reaction consists of the coupling of an α-bromo-ketone (**8**) with a 2-aminopyrimidine under microwave heating, followed by the addition of hydrazine. The application of this strategy to our compounds led to 2-amino-imidazole **9** at moderate yields (Scheme 2). The placing of the second alkene chain was then performed by acid coupling to form an amide (**10**). Finally, the ring closure metathesis reaction followed by direct hydrogenation of the resulting double bond led to macrocycle **11**.

BIOLOGY

Determination of the *in vitro* growth inhibitory activity of the 5-aryl-*1H*-imidazoles. We used an MTT colorimetric assay to evaluate the *in vitro* growth inhibitory effects of the 48 compounds synthesized and listed in Table 1. These *in vitro* growth inhibitory effects were determined in each cancer cell line by calculating the concentration that decreased the growth of this cancer cell line by 50% after 72 h of culture in the presence of the drug of interest (the IC_{50} *in vitro* growth inhibitory index, SI Table 1). This assay was performed on various cancer cell lines that we analyzed based on their display of sensitivity or resistance to pro-apoptotic stimuli. Four cancer cell lines displaying sensitivity to pro-apoptotic stimuli were thus analyzed: the mouse B16F10 melanoma,[24] the human prostate PC-3, [25] the breast MCF-7,[25] and the colon LoVo[26] carcinoma cell lines. In the same manner, four human cancer cell lines that displayed various levels of resistance to pro-apoptotic stimuli were also analyzed: the human U373[27, 28] and T98G glioma[27] the SKMEL-28 melanoma[24] and the A549 non-small cell lung carcinoma (NSCLC) [29] cell lines (SI Table 1).

Among the 48 compounds tested, the IC_{50} value range included non-active compounds (defined by mean IC_{50} values > 100 µM) to compounds with single digit µM IC_{50} values. No correlation between the IC_{50} values and calculated log P values could be found (see the SI).

Interestingly, the most active compounds, i.e., **2h**, **2i**, **2q**, **2r** and **2z,** displayed similar *in vitro* growth inhibitory activity in the various cancer cell lines analyzed regardless of the cell line level of resistance to pro-apoptotic stimuli (Table 1). Thus, it is unlikely that the *in vitro* growth inhibitory effects of this group of compounds related to pro-apoptotic effects, a hypothesis that we experimentally investigated as detailed below.

The mean IC_{50} concentration on cancer cells lines of **2i** (6µM) chosen among the 5 most potent compounds was further compared to its IC_{50} concentrations determined on immortal and primary non-cancerous cell lines. While immortal cells were as sensitive to **2i** as cancer cells (data not shown), NHDF and NHLF normal fibroblasts revealed to be 6 and 4 times less sensitive to **2i** respectively (NHDF: IC_{50} =36µM; NHLF: IC_{50}=22µM). This result indicates that **2i** could display some bioselectivity towards highly proliferative and metabolically active cells.

2i **displays cytostatic and not cytotoxic anti-cancer effects in melanoma cells.** We made use of computer-assisted phase-contrast microscopy (quantitative videomicroscopy) to study the effects of **2i** on two melanoma cell lines, i.e. the apoptosis-sensitive B16F10 mouse model and the apoptosis-resistant SKMEL-28 human model [24] at their respective IC_{50} *in vitro* growth inhibitory concentrations as determined by means of a colorimetric MTT assay. While the global growth of each of these two melanoma cell populations (SKMEL-28, Fig. 1A; B16F10, data not shown) was decreased by approximately 50% between 48 h and 72 h of culture (Fig. 1B), no cell death occurred according to the morphological analyses provided by quantitative videomicroscopy (Fig. 1A). In contrast, morphological changes emphasizing increases in cell size were observed, and **2i** displayed cytostatic rather than

cytotoxic effects (Fig. 1A). These results were further confirmed by flow cytometry determination of

cell cycle kinetics (Fig. 1C) and activation of apoptosis (Fig. 1D). Indeed, the data in Fig. 1C reveal that

2i did not modify the cell cycle kinetic profiles or activate apoptosis (Fig. 1D) in human SKMEL-28

melanoma cells. Similar results were obtained with the B16F10 melanoma cells (data not shown). The

fact that no significant modifications were observed in B16F10 and SKMEL-28 melanoma cell cycle

kinetics suggests that the **2i**-induced cytostatic effects are unrelated to a specific cell cycle phase.

Evaluation of the *in vitro* growth inhibitory concentration of 2i in the NCI 60 cancer cell line

panel. Compound **2i** was analyzed by the *National Cancer Institute* in a panel of 60 cancer cell lines at

10 µM (Fig. 2, revealed with the permission of the NCI). The data obtained revealed that the residual

growth ranged between 13 to 106% depending on the cell line analyzed (Fig. 2). The NCI 50% growth

inhibitory concentration determination using the 60 models equals 4 µM, a value which fits perfectly

with our data above (6 µM, Table 1).

We then compared the **2i** *in vitro* growth inhibitory response profiles of the NCI panel of 60 cancer cell

lines to the full NCI database compound profile set using the COMPARE algorithm developed by the

NCI [30, 31] as we have successfully done with other types of compounds.[32] We wanted to thus determine

the "Compare Correlation Coefficients" (the CCC index) with respect to the > 763,000 compounds

already present in the NCI database. The best CCC index we obtained was below 0.7, suggesting that

the mechanisms of action of **2i** as a potential anticancer agent should be distinct from those mechanisms

of action, at least in terms of *in vitro* cancer cell growth inhibition, of the > 763,000 compounds already

present in the NCI database.

Transcriptomic comparison of melanoma primary cultures that display different sensitivity levels

to *2i* highlights the mitochondria as a potential target for this compound. Because our group is

interested in identifying novel types of compounds to overcome, at least partly, the intrinsic resistance

of melanoma cells to cytotoxic compounds in general and to pro-apoptotic compounds in particular, we

had developed a collection of human melanoma primary cultures characterized at their genomic and

transcriptomic levels that we decided to use as further explained in the discussion to try to decipher, at

least partly the mechanism(s) by which **2i** exerts its growth inhibition. The IC_{50} growth inhibitory

concentrations of **2i** on the 11 previously characterized human melanoma primocultures[33] appeared to be

as heterogeneous (Fig. 3) as the *in vitro* profiling results conducted using the NCI panel of 60 cell lines

(Fig. 2). Thus, this panel of 11 melanoma primocultures did not modify the conclusions that could be

drawn from the NCI 60 cell line panel in terms of **2i**-induced *in vitro* growth inhibition of cancer cells.

The *in vitro* growth inhibition profiling of **2i** on this panel of 11 primocultures revealed that three cell

lines appeared rather resistant (VM-1, VM-23 and VM-30 cell lines further labeled as group 1; mean

$IC_{50} \pm SEM: >86 \pm 11$ µM), while 5 cell lines were more sensitive (VM-7, VM-8, VM-21, VM-24 and

VM-47; further labeled group 2; mean $IC_{50} \pm SEM = 6 \pm 2$ µM) when comparing the mean IC_{50} value

calculated for these 11 models, i.e., approximately 35 µM (the dotted line in Fig. 3). Using the Agilent

mRNA array-related data already available for these 11 primary melanoma cultures, [33] we proceeded

with bioinformatic comparison between groups 1 and 2 at the gene mRNA expression level to identify

potential genes that could explain, at least partly, the difference in sensitivity observed for **2i** in terms of

in vitro growth inhibition of these 11 melanoma primocultures.

As the up/down-regulated gene lists were quite extensive, we performed enrichment analysis using

EASE software.[34] It appeared that mitochondrial oxido-reductive metabolism could drive **2i**-induced *in*

vitro growth inhibition of cancer cells. We only took into account EASE scores with p values < 0.005

(Table 2). Indeed, both the cellular component categories and the biological processes that differentiate

the high (group 2) from the low (group 1) responsive melanoma cell lines to **2i** relate to the

mitochondria and, more particularly, to its inner membrane with a focus on the energetic pathways and

oxido-reductase activity (Table 2). The gene list symbols, names and functions are detailed in SI Table 2 as provided by the EASE annotation system.

Interestingly, group 1 cell lines, which are less sensitive to compound **2i,** generally overexpress these genes at the mRNA level. Therefore, it appears that mitochondrial activity could drive the **2i** response, and we experimentally checked this hypothesis as detailed below.

Evaluation of the effects of *2i* on mitochondria in SKMEL-28 melanoma cells. The mitochondria in untreated and **2i**-treated cells were visualized by fluorescent microscopy using MitoTracker®. Fig. 4A illustrates the typical morphological distribution and fluorescence intensity of SKMEL-28 cells left untreated or treated for 24 h with 5 µM **2i**. No major modification could be observed while an increase in cell size was again observed (see Fig. 1). Further analyses revealed that **2i** treatment induced a time-dependent increase in the oxygen reactive species content of the cells as shown in Fig. 4B. To validate that **2i** targets the mitochondrial metabolism, we made use of oxygraphic measurement. Interestingly, the direct addition of 10 µM **2i** compound in the oxygraphic chamber containing SKMEl-28 cells has no impact on the cellular oxygen consumption (data not shown), while pretreatment of SKMEL-28 cells for 72 h with 10 µM **2i** induced a marked increase in the subsequent oxygen consumption. These results were confirmed in the U373 apoptosis-resistant glioma model (data not shown). Thus, it appears that **2i** affects mitochondrial metabolism in an indirect manner, the mechanism of which remains to be deciphered.

DISCUSSION AND CONCLUSIONS

The panel of 48 compounds synthesized and tested in the current study allows some conclusions to be drawn concerning structure-activity relationships (Fig 5). First, the non-cyclized compounds (**2** and **10**) were systematically more active than their respective macrocyclic structure (**1, 7** and **11**). The aryl group

is found to be crucial for the biological activity since compound **14** which misses this motif shows no or a very low growth inhibition activity. The displacement of the aryl group in position 4 of the imidazole (see compound **15**) is also detrimental to the biological activity. Concerning the substitution pattern, the obtained IC_{50} for compounds **1b-f,h** and **2b-f,h,r-w** indicate that substitution of the aryl group (R^3, R^4 and/or $R^5 \neq H$) leads to a decrease of inhibition activity (except for $R^3 = i$-Pr, **2r**, which has no significant effect on the activity). The nature of the R^2 chain does not significantly influence the biological activity, as compounds with a methyl group in that position ($R^2 = CH_3$) presented similar activities to those possessing a longer chain (compare for instance **2i** and **2q**) (Fig. 5).

In contrast, the nature of substituent in position 2 of the imidazole (R^1) appears to have marked impact on the growth inhibition activity in cancer cell line models. Indeed, variations in the chain length (see **2a,g,i-j**) induce large difference in IC_{50}, with an optimal chain length of six carbon atoms ($R^1 = (CH_2)_4CH=CH_2$) (Fig. 5). The inclusion of fluorine (**2n**) or oxygen (**2y**) atoms in this alkene chain (R^1) is detrimental to its activity. However, the terminal unsaturation is important for activity (compare, for instance, **2k,l,o,x** with **2a,g,i-j,m,p,q,z,aa**), with the best results being obtained with a terminal double bond or a phenyl group (**2a-j,p-w,z,aa**) (Fig. 5).

The synthesis and biological evaluation of amide derivatives **10** and **11** indicated that 2-alkoxy and 2-amido imidazole derivatives possess very similar inhibition activities (compare **10** with **2i**).

Biological evaluations of one of the most active compounds, **2i,** indicated a potential First In Class molecule, at least when comparing its *in vitro* growth inhibitory profiles in 60 cancer cell lines with the >763,000 NCI molecule database. We obtained a COMPARE correlation coefficient < 0.7. To attempt to partly decipher the mechanism of action through which **2i** induces *in vitro* growth inhibitory activity in cancer cells, we made use of genetically well-defined models as previously done by other groups.[35-37] In the present study, we compared the transcriptomic characterization of highly versus less sensitive

melanoma models to compound **2i,** and this approach enabled us to highlight the mitochondria as a potential target candidate for **2i**. Indeed, the gene set enrichment analysis revealed 43 genes coding for proteins related to mitochondrial location (27/43 proteins, 10/27 mitochondrial membrane-related proteins) and/ or energetic and redox balance (31/43 proteins), two biological processes in which mitochondria play key roles (Table 2; SI table 2). Such mitochondria targeting is of clinical interest. Indeed, the targeting of the electron transfer chain (ETC) in the mitochondria by elesclomol produced therapeutic benefits in a phase II clinical trial in melanoma patients. [38] The experimental data that led to these clinical trials were obtained by using homozygote mutated yeast strain comparisons between sensitive and resistant models.[37]

The reprogramming of mitochondrial metabolism in cancer cells has been studied since 1923 when Otto Warburg described the aerobic glycolysis of these cells,[39] but no single compound on the market to date is known to specifically target this organelle function. This reprogramming has been recognized as one of the hallmarks of cancer[19] candidates for anti-cancer targeting to avoid, as best at least, non-specific adverse effects due to effects on normal cells.[40] In cancer cells and in melanoma in particular, the tricarboxylic acid Krebs (TCA) cycle is decoupled from glycolysis,[41] which produces approximately 50% of the needed ATP, while the remaining 50% is provided through the TCA cycle fed with other carbon sources than glucose, such as glutamine in particular.[41, 42] This decoupling is favorable for biosynthesis, energetic and redox balances. The equilibrium results of the balance between production and scavenging of ROS. Production is mainly due to the 1 to 4% of oxygen in the electron transfer chain that is incompletely reduced in $O_2^{\cdot-}$ and further in H_2O_2, while scavenging is performed by the four anti-oxidant defenses, glutathione oxidases and glutaredoxins that use reduced glutathione as an electron donor and the thioredoxins and peroxiredoxins that use NADPH as an electron donor.[40, 43] The equilibrium level of cancer cells is known to be higher compared with normal cells, making cancer cells more sensitive to oxidative stress.[40] Here, we demonstrated that **2i** treatment for 72 h induced an

increased respiration rate and, more precisely, O_2 consumption rates along with marked ROS production (Figure 4). These results fit with our findings that the expression levels of genes of the ETC, e.g. COX5B, COX6C, COX17, FDXR, NDUFA5, and NDUFA6 and more generally of the oxido-reductase balance, i.e., ACADS, AMID, BLVRB, COX5B, COX6C, DECR1, FADS2, FDXR, FLJ10661, FMO4, HSD17B12, IDH3A, MDH1, NDUFA5, NDUFA6, QDPR, RRM2B, SEPW1, TXN, UQCRB, and VAT1, are associated with differences in **2i**-mediated *in vitro* growth inhibitory activities (Table 2; SI Table 2). Such a high metabolic rate and mitochondrial dysfunction can lead to increased ROS production and inefficient ATP generation. Because cancer cells display increased energy needs, the perturbation of mitochondrial respiration and/or of glycolysis is an attractive avenue when developing new drugs. The sensitization of cancer cells to death has already been shown with metformin, which inhibits oxidative phosphorylation, and with 2-deoxyglucose or lonidamine, which inhibit hexokinase.[44] Moreover, the oxidation status of cysteine residues of proteins regulates the duration and intensity of transduction signals to the nucleus. Interestingly, the signaling pathways modulated by glutathione and thioredoxins are not the same, and the outcome of this regulation will depend on the local context.[45] Increased levels of ROS can thus lead to apoptosis, cell cycle deregulation, senescence or tumorigenesis. Indeed, the cell cycle has been shown to be synchronized with the respiration cycle through the oxidative status tuning of the PI3K/Akt/FoxO3a pathway.[45] In the present study, we demonstrated that disruption of mitochondrial functions and increased intracellular ROS content is associated with cytostatic effects in cancer cells (Figure 1). Therefore, our compound differs from elesclomol, which induces apoptosis as a consequence of massive ROS production through ETC perturbation that depends directly on its copper-binding properties.[37] As **2i** treatment does not directly alter O_2 consumption, we hypothesize the existence of indirect and different mechanisms of action than those observed with elesclomol and that remain to be deciphered.

In conclusion, we have synthesized forty-eight 5-aryl-1*H*-imidazoles, among which several compounds displayed single digit μM 50% growth inhibitory concentration against various cancer models, including apoptosis-resistant ones such as melanomas. Interestingly, the mechanism by which these compounds (at least **2i**) exert their anti-cancer cytostatic activities does not correlate with any compound from the NCI database. In contrast, we discovered that these compounds could induce perturbations of mitochondrial energetic metabolism, leading to increased O_2 consumption and reactive oxygen species production. Because this metabolism is known to be reprogrammed in cancer cells, these compounds could represent a new way to combat apoptosis-resistant cancer types.

EXPERIMENTAL SECTION

CHEMISTRY

Flash chromatography was performed on silica gel (230-400 mesh). TLC was performed on aluminum-backed silica plates that were developed using standard visualizing agents: UV fluorescence (254 and 366 nm), $KMnO_4$. NMR spectra were recorded at 300 or 500 MHz for ^{1}H NMR and at 75 MHz for ^{13}C NMR. Chemical shifts (δ) are given in part per million downfield from internal TMS. Reactions under microwave heating were conducted in a sealed tube using MicroSYNTH equipment (Milestone Srl). The temperature of the reaction mixture was monitored via an infrared sensor. Infrared spectra were recorded using a Shimadzu FTIR-8400S spectrometer. Mass spectra were recorded using a Finnigan MAT LCQ mass spectrometer. HRMS were recorded by the MAPS laboratory at the University College of London. The synthesis and characterization of compounds **1a-e,g,i-j**, **2a-e,g,i-j**, **6a-b** and **7a** have been previously reported.[18, 20, 21] The general procedures and key analytical data for **1i** are reported below with full data for all derivatives in the Supporting Information. The purity of intermediates was measured by ^{1}H and ^{13}C NMR. The purity of the final compounds was determined by analytical reverse-HPLC (Xbridge C18). The measured purity was >95%.

General procedure for alkylation of bromophenols. DBU (9.70 mmol, 1.5 equiv) was added dropwise to a solution of corresponding bromophenol (6.47 mmol, 1 equiv) in DMF (10 ml). The mesylate (8.415 mmol, 1.3 equiv) was added dropwise to this solution and then the *t*-butylammonium iodine (0.198 mmol, 0.03 equiv). The mixture was heated at 70°C for 7 hours and then stirred at room temperature overnight. The solvent was evaporated under reduced pressure. Ether (100 mL), water (15 ml) and a solution of HCl 1 N (5 mL) were added. The phases were separated, and the organic phase was washed with water (2×20 mL). The combined aqueous phases were extracted with ether (2×30 mL). The organic phases were collected, dried (MgSO$_4$), and concentrated in vacuo.

Characterization of 2-bromo-1-(hex-5-en-1-yloxy)benzene (12a)

Colorless oil; Yield: 1.47 g (91%); ^{1}H NMR (300 MHz, CDCl$_3$): δ 7.53 (dd, 1H, J =1.6, 7.9 Hz), 7.24 (ddd, 1H, J = 1.6, 7.4, 8.3 Hz), 6.88 (dd, 1H, J = 1.3, 8.3 Hz), 6.82 (dt, 1H, J = 1.4, 7.6 Hz), 5.89-5.78 (m, 1H), 5.01-4.99 (m, 2H), 4.03 (t, 2H, J = 6.4 Hz), 2.20-2.10 (m, 2H), 1.90-1.80 (m, 2H), 1.70-1.60 (m, 1H); ^{13}C NMR (75 MHz, CDCl$_3$): δ 155.6, 138.7, 133.5, 128.5, 121.8, 114.9, 113.3, 112.4, 69.1, 33.5, 28.7, 25.4; IR: 3074, 2941, 2858, 1535, 1500, 1491, 1369, 1244, 1142, 912 cm^{-1}; CI-MS m/z: 254; HRMS calcd for C$_{12}$H$_{15}$O[79]Br: 254.0301, found: 254.0314.

General procedure for the synthesis of boronic acids. The corresponding alkylated bromophenol (4.68 mmol, 1 equiv) in THF (20 ml) was cooled down to -78°C. *n*-BuLi (2.5 M in hexane, 6.24 mmol, 1.3 equiv) was added dropwise. The mixture was stirred at -78°C for 1 hour and then the triisopropyl borate (9.35 mmol, 2 equiv) was added dropwise. The mixture was stirred overnight. Ethyl acetate (10 ml) and an aqueous solution of HCl 1 N (7 ml, until pH = 1) were added. The phases were separated, and the combined aqueous phases were extracted with ethyl acetate (3× 20 mL). The organic phases were collected, dried (MgSO$_4$), and concentrated in vacuo. The crude product was purified by flash chromatography over silica with a mixture of cyclohexane/ethyl acetate as an eluent.

Characterization of 2-(hex-5-en-1-yloxy)phenylboronic acid (3a)

Colorless oil; Yield: 945 mg (84 %); ^{1}H NMR (300 MHz, CDCl$_3$): δ 7.87 (dd, 1H, *J* = 7.3, 1.7 Hz), 7.45-7.40 (m, 1H), 7.03 (t, 1H, *J* = 7.3 Hz), 6.90 (d, 1H, *J* = 8.3 Hz), 6.04 (s, 2H), 5.89-5.75 (m, 1H), 5.08-4.98 (m, 2H), 4.09 (t, 2H, *J* = 6.6 Hz), 2.19-211 (m, 2H), 1.90-1.80 (m, 2H), 1.65-1.55 (m, 2H); ^{13}C NMR (300 MHz, CDCl$_3$): δ 164.1, 138.2, 137.0, 132.9, 121.3, 115.3, 110.9, 68.3, 33.4, 28.7, 25.4; IR: 3409, 3074, 2926, 2854, 1641, 1599, 1576, 1487, 1448, 1340, 1225, 910 cm^{-1}; CI-MS m/z: 220, 219; HRMS calcd for C$_{12}$H$_{17}$BO$_3$: 220.1265, found: 220.1265.

General procedure for S$_N$Ar: alcohol (10.40 mmol, 5 equiv) was added to a solution of sodium hydride (60 wt% suspension in mineral oil, 9.58 mmol, 4.6 equiv.) in dry THF (7 mL), under argon. The solution was stirred until no more gas evolution was observed and then added to a solution of 1-methyl-5-iodo-2-phenylsulfonylimidazole (**5**) (2.08 mmol, 1 equiv.) in dry THF (35 mL). The reaction mixture was transferred into a sealed tube and heated with microwaving for 8 h at 80 °C. Ethyl acetate (50 mL) and saturated sodium chloride solution (30 mL) were successively added. The organic phase was further washed twice with a saturated sodium chloride (30 mL). The combined aqueous phases were extracted with ethyl acetate (20 mL). The combined organic phases were dried over MgSO$_4$, and concentrated under reduced pressure. The crude product was purified by flash chromatography over silica using a mixture of hexane/ethyl acetate as eluent.

Characterization of 5-iodo-1-methyl-2-(hex-4-en-1-yloxy)-1*H*-imidazole (4a)

Yellow oil; Yield : 402 mg were obtained from 0.6 g of **5** (76 %); ^{1}H NMR (300 MHz, CDCl$_3$): δ 6.73 (s, 1H), 5.87-5.74 (m, 1H); 5.05-4.95 (m, 2H); 4.32 (t, 2H, *J* = 6.5 Hz), 3.33 (s, 3H), 2.15-2.05 (m, 2H), 1.83-1.74 (m, 2H), 1.57-1.48 (m, 2H); ^{13}C NMR (75 MHz, CDCl$_3$): δ 154.0, 138.6, 130.4, 115.1, 69.8, 63.7, 33.5, 31.4, 28.7, 25.3; IR: 3074, 2937, 2858, 1541, 1496, 1475, 1253, 1142, 910 cm^{-1}; ESI-MS m/z: 307; HRMS calcd for C$_{10}$H$_{16}$IN$_2$O: 307.0307, found: 307.0298.

General procedure for Suzuki coupling: Tetrakis (triphenylphosphino) palladium (0.012 mmol, 0.03

equiv.) and **4** (0.342 mmol, 1 equiv.) in dimethoxyethane (4 mL) were introduced in a microwave tube.

Boronic acid (**3**) (0.376 mmol, 1.1 equiv.) in dimethoxyethane (4 mL), water (4 mL), and an aqueous

solution of sodium carbonate (20%, 3 equiv.) were successively added. The resulting mixture was then

degassed for 30 min by means of a flow of argon and placed in a microwave oven at 105 °C and 200 W

for 1 h. Ethyl acetate (100 mL) and water (50 mL) were added. The phases were separated, and the

aqueous phases were extracted with ethyl acetate (50 mL). The organic phases were combined, washed

with a saturated aqueous solution of NaCl (50 mL), dried over $MgSO_4$, and concentrated under reduced

pressure. The crude product was purified by flash chromatography using CH_2Cl_2/2-propanol 97/3 as an

eluent.

Characterization of 2-(hex-3-en-yloxy)-5-[2-(hex-5-en-1-yloxy)phenyl]-1-methyl-1*H*-imidazole (2i)

Yellow oil; Yield: 166 mg were obtained from 235 mg of **12'** (76 %); ^{1}H NMR (300 MHz, $CDCl_3$):

δ 7.32 (td, 1H, J = 8.1, 1.8 Hz), 7.25 (dd, 1H, J = 8.1, 1.8 Hz), 6.97 (dt, 1H, J = 7.4, 0.9 Hz), 6.94 (d,

1H, J = 8.1 Hz), 6.61 (s, 1H), 5.90-5.71 (m, 2H); 5.07-4.94 (m, 4H); 4.38 (t, 2H, J = 6.7 Hz), 3.97 (t,

2H, J = 6.6 Hz), 3.25 (s, 3H), 2.18-2.02 (m, 4H), 1.88-1.70 (m, 4H), 1.62-1.42 (m, 4H); ^{13}C NMR (75

MHz, $CDCl_3$): δ 157.0, 153.7, 138.8, 138.7, 132.2, 129.8, 126.7, 121.8, 120.9, 120.2, 115.1, 112.4, 69.5,

68.5, 33.7, 33.6, 29.7, 28.92, 28.87, 25.52, 25.51; IR: 3074, 2935, 2858, 1639, 1580, 1497, 1244, 1142,

995, 800 cm^{-1}; ESI-MS m/z: 355; HRMS calcd for $C_{22}H_{31}N_2O_2$: 355.2386, found: 355.2374.

General procedure for RCM reaction. Imidazole **2** (0.266 mmol, 1 equiv) and 1,2-dichloromethane

(70 ml) were introduced in a flask under argon. The mixture was heated at 95°C (reflux). A Grubbs

catalyst (second generation) (0.013 mmol, 0.05 equiv) was added. After one day, a second fraction of

Grubbs catalyst (0.007 mmol, 0.025 equiv) was added, and the solution was stirred at reflux for 24

hours. The mixture was cooled down until room temperature and potassium isocyanate (20 mg) was

added. After one hour of stirring, the solvent was evaporated. The crude product was filtrated by flash chromatography over silica with a mixture of cyclohexane/ethyl acetate as an eluent and directly engaged to the next step.

General procedure for hydrogenation. Imidazole **7** (0.44 mmol, 1 equiv), ethanol (10 ml) and ethyl acetate (10 ml) were added in a flask. The catalyst Pd/C 10% (0.0222 mmol, 0.05 equiv.) was added and the mixture was placed under $H_2(g)$ atmosphere. After 2 h 30, the mixture was filtrated and concentrated under vacuum. The crude product was purified by flash chromatography over silica with a mixture of cyclohexane/ethyl acetate as an eluent.

Characterization of 23-methyl-8,19-dioxa-21,23-diazatricyclo[18.2.1.0²,⁷]tricosa-1(22),2,4,6,20-pentaene (1i)

Colorless oil; Yield : 106 mg were obtained from 145 mg of **7i** (49 % over the two steps; purity = 90%); ^{1}H NMR (300 MHz, CDCl$_3$): δ 7.34 (td, 1H, J = 7.7, 1.8 Hz), 7.27 (dd, 1H, J = 7.4, 1.8 Hz), 6.98 (dt, 1H, J = 7.4, 1.0 Hz), 6.92 (d, 1H, J = 8.2 Hz), 6.56 (s, 1H), 4.81 (dt, 1H, J = 10.5, 2.9 Hz); 4.20 (dt, 1H, J = 7.1, 2.9 Hz), 4.00-3.96 (m, 1H); 3.88 (dt, 1H, J = 7.7, 3.0 Hz,), 3.23 (s, 3H), 1.98-1.91 (m, 1H), 1.80-1.60 (m, 4H), 1.58-1.20 (m, 11H); ^{13}C NMR (75 MHz, CDCl$_3$): δ 157.6, 153.3, 132.4, 130.2, 126.8, 121.2, 121.0, 120.4, 112.4, 69.7, 69.0, 29.7., 29.5, 28.6, 28.2; 28.1, 27.6, 27,4, 26,4, 25.9; IR: 2927, 2854, 1579, 1537, 1492, 1448, 1377, 1244, 1142, 1053, 991, 800 cm^{-1}; ESI-MS m/z: 329; HRMS calcd for C$_{20}$H$_{29}$N$_2$O$_2$: 329.2229, found: 329.2231.

General procedure for the formation of fumaric salts. The imidazole compound (1 equiv.) was dissolved in ethanol (0.1 M). A solution of fumaric acid (1 equiv.) in ethanol (0.05 M) was added. The mixture was stirred overnight and then concentrated under reduced pressure. The correct 1:1 ratio was verified by ^{1}H NMR.

BIOLOGY

Cell lines and compounds. Seven human and one mouse cancer cell lines were obtained from either the European Collection of Cell Cultures (ECACC; Salisbury, UK) or the American Type Culture Collection (ATCC; Manassas, VA). The two glioma cell lines were the U373 (ECACC code 89081403) and T98G (ATCC code CRL-1690) astroglioma cell lines. The carcinoma cell lines were the A549 non small cell carcinoma cell line (ATCC code CCL185), the MCF-7 mammary breast carcinoma cell line (ATCC code HTB-22), the Lovo colon cancer cell line (ATCC code CCL-229) and the PC-3 prostate cancer cell line (ATCC code CRL-1435). The melanoma cell lines were the mouse B16F10 cells (ATCC code CRL-6475) and the human SKMEL-28 cells (ATCC code HTB-72). The two immortal non-cancerous cell lines were the HBL100 human breast epithelial cells (330178) and the HaCat human keratinocyte cells (300493) that were purchased from Cell Lines Service (Eppelheim, Germany). The two human normal primary cell lines were from fibroblast origin (NHDF and NHLF: normal human dermal fibroblasts and normal human lung fibroblasts respectively; codes CC-2509 and CC-2512) and were purchase from Lonza (Braine L'Alleud, Belgium).

The human melanoma primary cultures were obtained as previously described with full genomic and transcriptomic characterization.[33]

All biological assays were performed on fumaric salts (see above).

Determination of the IC$_{50}$ growth inhibitory concentration. We made use of a colorimetric MTT assay to determine the concentration that reduced the whole cell population by 50% after 72 h of exposure to the compound as described previously.[32] This test is based on the ability of living cells to reduce 3-(4,5-dimethylthiazol-2-yl)-2,5-diphenyl tetrazolium bromide (MTT) salt in purple formazan crystals via mitochondrial succinate dehydrogenase enzymatic activity. Each experimental condition was run in six replicates.

Quantitative videomicroscopy. The effects of tested compounds on cell morphology, cell proliferation and cell death were assessed with the global view system developed in our lab and described previously.[32, 46] Briefly, each cell culture field was photographed every 4 minutes over a 72-h period to be compressed in a short 1-minute movie. Global growth (GG) is the ratio between the number of cell present on the picture at one time point and the number of cell present at time 0. Each condition was tested in three replicates. The global growth ratio (GGR) is calculated by dividing the treated global growth value by the global growth value of the control condition. In that case, the control GGR is 1.

Flow cytometry

Apoptosis and cell cycle profile analyses. The **2i**-induced effects on cell cycle kinetics and apoptosis were evaluated by means of flow cytometry with the double propidium iodide and TUNEL staining by using the APO-Direct™ kit according to the manufacturer instructions (BD Biosciences, Erembodegem, Belgium) as described previously.[47]

Intracellular reactive oxygen species measurements. DCFH-DA (2'-7'-dichlorodihydrofluorescein diacetate, Sigma-Aldrich, Bornem, Belgium) is a cell-permeant indicator for reactive oxygen species (ROS). This chemically reduced and acetylated form of DCF, once inside the cell, is deacetylated by intracellular esterases that yield the dye retained intracellularly in a charged form. The oxidation of this later probe by ROS can be detected by monitoring the increase in fluorescence by flow cytometry.

Briefly, after cell exposure to the drug, the cells are washed twice and stained for 1 h at 37°C with 20 μM DCFH-DA in RPMI without phenol red medium.[48] After two washing steps, cells are detached by trypsin and fluorescence was measured with a Cell Lab Quanta cytometer (Beckman Coulter, Analis, Suarlée, Belgium). The experiments were conducted once in quadruplicate.

Mitochondria fluorescent staining. We made use of MitoTracker® Green FM (Invitrogen, Merelbeke, Belgium) to highlight mitochondria. Briefly, SKMEL-28 cells were seeded on glass coverslips 48 h

before treatment with **2i** at 5 µM for 3 to 48 h. After two washing steps, the mitochondria were stained

with 100nM of MitoTracker® Green FM in RPMI without phenol red for 30 min. After two rinses, the

cells were visualized under a Zeiss Axio fluorescent microscope (Zeiss, Oberkochen, Germany). Three

coverslips per experimental condition were analyzed.

Oxygraphy. The cellular ROUTINE respiration, reflecting the aerobic metabolic activity under routine

culture conditions (with the physiological substrates in culture medium) of SKMEl-28 and U373 cancer

cells were recorded by high-resolution respirometry with a Clark electrode, at 37 °C (OROBOROS

INSTRUMENTS, Innsbruck, Austria). The oxygraph was calibrated as recommended with the assay

Dulbecco Modified Eagle's Medium containing glucose (1 g/L) and pyruvate (110 mg/L) without

phenol red (Gibco, Invitrogen, Belgium). Five million cells, pre-incubated during the last 72 h with **2i**

(10^{-5} M) or not (control cells), diluted in assay medium, were transferred into each respiratory chamber

of the oxygraph. The measurement was performed under continuous stirring and started just after the

closing of the chamber. The slopes of O_2 consumption, representing the routine respiration of the cells,

were calculated with the Oroboros oxygraph software (DatLab 4.0, OROBOROS DatLab software,

Innsbruck, Austria). Data are presented in relative values (%) in reference to the control group, for

which the routine respiratory rate was considered 100%.

Bioinformatic analyses. We normalized the measured expression values via a multiplicative

transformation chosen so that approximately the same number of probes appeared relatively

overexpressed in each of the arrays. We evaluated the multiplicative factors using the whole array as

well as several subsets of probes and used this information to estimate uncertainties in expression due to

normalization.

After normalization, we scored probes according to their ability to separate low- and high response cell

lines. We adopted an order-based scoring system closely linked to the well-known Mann-Whitney

statistic. In contrast to the usual approach where a cell-line would be represented by a single number, we

used the normalized expression values together with their lower/upper uncertainty levels in the calculation. The addition of uncertainty information increases the resolution of the score and helps distinguish between marginally and strongly different expression levels, even in small group sizes. For groups with three and five cell lines, the scoring system allows for 135 distinct values. We reported them in a signed format with values ± 1 indicating perfect separation and higher absolute values indicating progressively worse separation.

We compiled a short list of genes by picking probes with absolute score values ≤ 5. Finally, we analyzed enrichment of the short gene lists in different Gene Ontology categories using the EASE (Expression Analysis Systematic Explorer) software package (version 2.0) as previously described.[32] Briefly, EASE ranks functional gene clusters by means of the statistical over-representation of individual genes in specific categories relative to all the genes in the same category on the microarray.

Supporting Information Available. Full analytical and spectral data for all synthesized compounds as well as tables of COMPARE analysis and bioinformatic comparisons' data between group 1 and 2. This material is available free of charge via the Internet at http://pubs.acs.org.

Corresponding authors' informations

*V Mathieu (biology): Phone: +32-2-6505179. E-mail: vemathie@ulb.ac.be ; R Robiette (chemistry): Phone: +32-10-479176. Fax: +32-10-474168. E-mail: raphael.robiette@uclouvain.be.

Abbreviations

DBBA = 5,5-dibromobarbituric acid

MW = microwave heating

REFERENCES

(1) Talbäck, M.; Stenbeck, M.; Rosén, M.; Barlow, L.; Glimelius, B. Cancer survival in Sweden 1960-1998--developments across four decades. *Acta Oncol*. **2003**, *42*, 637-659.

(2) Verdecchia, A.; Francisci, S.; Brenner, H.; Gatta, G.; Micheli, A.; Mangone, L.; Kunkler, I. EUROCARE-4 Working Group. Recent cancer survival in Europe: a 2000-02 period analysis of EUROCARE-4 data. *Lancet Oncol*. **2007**, *8*, 784-796. Erratum in: *Lancet Oncol*. **2008**, *9*, 416.

(3) Chen, K.G.; Sikic B. I. Molecular pathways: regulation and therapeutic implications of multidrug resistance. *Clin Cancer Res*. **2012**, *18*, 1863-1869.

(4) Wilting, R. H.; Dannenberg J. H. Epigenetic mechanisms in tumorigenesis, tumor cell heterogeneity and drug resistance. *Drug Resist Updat*. **2012**, *15*:21-38.

(5) Wilson, T. R.; Johnston, P. G.; Longley, D. B. Anti-apoptotic mechanisms of drug resistance in cancer. *Curr. Cancer Drug Targets* **2009**, *9*, 307-319.

(6) Wong, R. S. Apoptosis in cancer: from pathogenesis to treatment. *J. Exp. Clin. Cancer Res*. **2011**, *30*:87.

(7) Savage, P.; Stebbing, J.; Bower, M.; Crook, T. Why does cytotoxic chemotherapy cure only some cancers? *Nat. Clin. Pract. Oncol*. **2009**, *6*, 43-52.

(8) Lefranc, F.; Brotchi, J.; Kiss, R. Possible future issues in the treatment of glioblastomas, with a special emphasis on cell migration and the resistance of migrating glioblastoma cells to apoptosis. *J. Clin. Oncol*. **2005**, *23*, 2411-2422.

(9) Soengas, M. S.; Lowe, S. W. Apoptosis and melanoma chemoresistance. *Oncogene* **2003**, *22*, 3138-3151.

(10) La Porta, C. A. Mechanism of drug sensitivity and resistance in melanoma. *Curr Cancer Drug Targets*. **2009**, *9*, 391-397.

(11) Han, S.; Roman, J. Targeting apoptotic signaling pathways in human lung cancer. *Curr. Cancer Drug Targets* **2010**, *10*, 566-574.

(12) Sugerman, P. B.; Joseph, B. K.; Savage, N. W. Review article: The role of oncogenes, tumour suppressor genes and growth factors in oral squamous cell carcinoma: a case of apoptosis versus proliferation. *Oral Dis*. **1995**, *1*, 172-188.

(13) D'Amico, T. A.; Harpole, D. H. Jr. Molecular biology of esophageal cancer. *Chest Surg. Clin. N. Am.* **2000**, *10*, 451-469.

(14) Wong, H. H.; Lemoine, N. R. Pancreatic cancer: molecular pathogenesis and new therapeutic targets. *Nat. Rev. Gastroenterol. Hepatol*. **2009**, *6*, 412-422.

(15) Bellina, F.; Cauteruccio, S.; Rossi, R. Synthesis and biological activity of vicinal diaryl-substituted 1*H*-imidazoles. *Tetrahedron* **2007**, *63*, 4571–4624.

(16) Bellina, F.; Cauteruccio, S.; Di Fiore, A.; Marchetti, C.; Rossi, R. Highly selective synthesis of 4(5)-aryl-,2,5(5)-diaryl-, and 4,5-diaryl-1*H*-imidazoles via Pd-catalyzed direct C-5 arylation of 1-benzyl-1*H*-imidazole. *Tetrahedron* **2008**, *64*, 6060-6072.

(17) Chen, J.; Ahn, S.; Wang, J.; Lu, Y.; Dalton, J. T.; Miller, D. D.; Li, W. Discovery of novel 2-aryl-4-benzoyl-imidazole (ABI-III) analogues targeting tubulin polymerization as antiproliferative agents. *J Med Chem*. **2012**, *55,* 7285-7289.

(18) Nshimyumukiza, P.; Van Den Berge, E.; Delest, B.; Mijatovic, T.; Kiss, R.; Marchand-Brynaert, J.; Robiette, R. Synthesis and biological evaluation of novel imidazole-containing macrocycles. *Tetrahedron.***2010**, *66*, 4515-4520.

(19) Hanahan, D.; Weinberg, R. A. Hallmarks of cancer: the next generation. *Cell* **2011**, *144*, 646-674.

(20) Delest, B. ; Nshimyumukiza, P. ; Fasbender, O.; Tinant, B.; Marchand-Brynaert, J.; Darro, F.; Robiette, R. Divergent and regioselective synthesis of 1,2,4- and 1,2,5-trisubstituted imidazoles. *J. Org. Chem.* **2008**, *73*, 6816-6823.

(21) Van Den Berge, E.; Pospisil, J.; Tran, T. V.; Collard, L.; Robiette, R. Planar chirality of imidazole-containing macrocycles- understanding and tuning atropoisomerism. *Eur. J. Org. Chem*. **2011**, 6649-6655.

(22) Ermolat'ev, D. S.; Abaev, E. V.; Van der Eycken, E. V. Efficient one pot, two step, microwave-assisted procedure for the synthesis of polysubstituted 2-aminoimidazoles. *Org. Lett.* **2006**, *8*, 5781-5784.

(23) Ermolat'ev, D. S.; Alifanov, V. L.; Rybakov, V. B.; Babaev, E. V.; Van der Eycken, E. V. A concise microwave-assisted synthesis of 2-aminoimidazole marine sponge alkaloids of the isonaamines series. *Synthesis* **2008**, *13*, 2083-2088.

(24) Van Goietsenoven, G.; Hutton, J.; Becker, J. P.; Lallemand, B.; Robert, F.; Lefranc, F.; Pirker, C.; Vandenbussche, G.; Van Antwerpen, P.; Evidente, A.; Berger, W.; Prévost, M.; Pelletier, J.; Kiss, R.; Kinzy, T. G.; Kornienko, A.; Mathieu, V. Targeting of eEF1A with Amaryllidaceae isocarbostyrils as a strategy to combat melanomas. *FASEB J*. **2010**, *24,* 4575-4584.

(25) Dumont, P.; Ingrassia, L.; Rouzeau, S.; Ribaucour, F.; Thomas, S.; Roland, I.; Darro, F.; Lefranc, F.; Kiss, R. The Amaryllidaceae isocarbostyril narciclasine induces apoptosis by activation of the death receptor and/or mitochondrial pathways in cancer cells but not in normal fibroblasts. *Neoplasia*. **2007**, *9,* 766-776.

(26) Yao, Y.; Jia, X. Y.; Tian, H. Y.; Jiang, Y. X.; Xu, G. J.; Qian, Q. J.; Zhao, F. K. Comparative proteomic analysis of colon cancer cells in response to oxaliplatin treatment. *BiochimBiophysActa*. **2009**, *1794*, 1433-1440.

(27) Branle, F.; Lefranc, F.; Camby, I.; Jeuken, J.; Geurts-Moespot, A.; Sprenger, S.; Sweep, F.; Kiss, R.; Salmon, I. Evaluation of the efficiency of chemotherapy in in vivo orthotopic models of human glioma cells with and without 1p19q deletions and inC6 rat orthotopic allografts serving for the evaluation of surgery combined with chemotherapy. *Cancer*, **2002**, *95,* 641-655.

(28) Ingrassia, L.; Lefranc, F.; Dewelle, J.; Pottier, L.; Mathieu, V.; Spiegl-Kreinecker, S.; Sauvage, S.; El Yazidi, M.; Dehoux, M.; Berger, W.; Van Quaquebeke, E.; Kiss, R. Structure-activity relationship analysis of novel derivatives of narciclasine (an Amaryllidaceae isocarbostyril derivative) as potential anticancer agents. *J Med Chem*, **2009**, *52,* 1100-1114.

(29) Mijatovic, T.; Mathieu, V.; Gaussin, J. F.; De Nève, N.; Ribaucour, F.; Van Quaquebeke, E.; Dumont, P.; Darro, F.; Kiss, R. Cardenolide-induced lysosomal membrane permeabilization demonstrates therapeutic benefits in experimental human non-small cell lung cancers. *Neoplasia.* **2006**, *8*, 402-412.

(30) Paull, K. D.; Shoemaker, R. H.; Hodes, L.; Monks, A.; Scudiero, D. A.; Rubinstein, L.; Plowman, J.; Boyd, M. R. Display and analysis of patterns of differential activity of drugs against human tumor cell lines: development of mean graph and COMPARE algorithm. *J. Natl. Cancer Inst.* **1989**, *81*, 1088−1092.

(31) Chan, J.; Khan, S. N.; Harvey, I.; Merrick, W.; Pelletier, J. Eukaryotic protein synthesis inhibitors identified by comparison of cytotoxicity profiles. *RNA* **2004,** *10*, 528−543.

(32) Frédérick, R.; Bruyère, C.; Vancraeynest, C.; Reniers, J.; Meinguet, C.; Pochet, L.; Backlund, A.; Masereel, B.; Kiss, R.; Wouters, J. Novel trisubstituted harmine derivatives with original in vitro anticancer activity. *J Med Chem.* **2012***, 55*, 6489-6501.

(33) Mathieu, V.; Pirker, C.; Schmidt, W. M.; Spiegl-Kreinecker, S.; Lötsch, D.; Heffeter, P.;Hegedus, B.; Grusch, M.; Kiss, R.; Berger, W. Aggressiveness of human melanoma xenograft models is promoted by aneuploidy-driven gene expression deregulation. *Oncotarget.* **2012**, *3,* 399-413.

(34) Le Mercier, M.; Mathieu, V.; Haibe-Kains, B.; Bontempi, G.; Mijatovic, T.; Decaestecker, C.; Kiss, R.; Lefranc, F. Knocking down galectin 1 in human hs683 glioblastoma cells impairs both angiogenesis and endoplasmic reticulum stress responses. *J Neuropathol Exp Neurol* **2008**, 67, 456-469.

(35) Gautam, P.; Upadhyay, S. K.; Hassan, W.; Madan, T.; Sirdeshmukh, R.; Sundaram, C. S.; Gade, W. N.; Basir, S. F.; Singh, Y.; Sarma, P. U. Transcriptomic and proteomic profile of Aspergillus fumigatus on exposure to artemisinin. *Mycopathologia*. **2011**, *172*, 331-346.

(36) Cui Y.; Paules, R. S. Use of transcriptomics in understanding mechanisms of drug-induced toxicity. *Pharmacogenomics*. **2010**, *11*, 573-585.

(37) Blackman, R. K.; Cheung-Ong, K.; Gebbia, M.; Proia, D. A.; He, S.; Kepros, J.; Jonneaux, A.; Marchetti, P.; Kluza, J.; Rao, P. E.; Wada, Y.; Giaever, G.; Nislow, C. Mitochondrial electron transport is the cellular target of the oncology drug elesclomol. *PLOS One*. **2012**, *7*: e29798.

(38) O'Day, S.; Gonzalez, R.; Lawson, D.; Weber, R.; Hutchins, L.; Anderson, C.; Haddad, J.; Kong, S.; Williams, A.; Jacobson, E. Phase II, randomized, controlled, double-blinded trial of weekly elesclomol plus paclitaxel versus paclitaxel alone for stage IV metastatic melanoma. *J Clin Oncol*. **2009**, *27*, 5452-5458.

(39) Warburg, O.Versuche am überlebenden Karzinomgewebe. *Biochem Z, 142*, 317-333.

(40) Montero, A.J.; Jassem, J. Cellular redox pathways as a therapeutic target in the treatment of cancer. *Drugs*. **2011**, *71*, 1385-1396.

(41) Filipp, F. V.; Ratnikov, B.; De Ingeniis, J.; Smith, J. W.; Osterman, A. L.; Scott, D. A. Glutamine-fueled mitochondrial metabolism is decoupled from glycolysis in melanoma. *Pigment Cell Melanoma Res*. **2012,** *25*, 732-739.

(42) Wenner, C. E. Targeting mitochondria as a therapeutic target in cancer. *J Cell Physiol*. **2012,** *227*, 450-456.

(43) Murphy, M. P. Mitochondrial thiols in antioxidant protection and redox signaling: distinct roles for glutathionylation and other thiol modifications. *Antioxid Redox Signal*. **2012,** *16*, 476-95.

(44) Indran, I. R.; Tufo, G.; Pervaiz, S.; Brenner, C. Recent advances in apoptosis, mitochondria and drug resistance in cancer cells. *Biochim Biophys Acta*. **2011,** *1807*, 735-745.

(45) Burhans, W. C.; Heintz, N. H. The cell cycle is a redox cycle: linking phase-specific targets to cell fate. *Free Radic Biol Med*. **2009**, *47*, 1282-1293.

(46) Debeir, O.; Mégalizzi, V.; Warzée, N.; Kiss, R.; Decaestecker, C. Videomicroscopic extraction of specific information on cell proliferation and migration in vitro. *Exp Cell Res*, **2008**, *314*, 2985-2998.

(47) Le Calvé, B.; Lallemand, B.; Perrone, C.; Lenglet, G.; Depauw, S.; Van Goietsenoven, G.; Bury, M.; Vurro, M.; Herphelin, F.; Andolfi, A.; Zonno, M. C.; Mathieu, V.; Dufrasne, F.; VanAntwerpen, P.; Poumay, Y.; David-Cordonnier, M. H.; Evidente, A.; Kiss, R. In vitro anticancer activity, toxicity and structure-activity relationships of phyllostictine A, a natural oxazatricycloalkenone produced by the fungus Phyllostictacirsii. *Toxicol Appl Pharmacol*, **2011**, *254*, 8-17.

(48) Gnoula, C.; Mégalizzi, V.; De Nève, N.; Sauvage, S.; Ribaucour, F.; Guissou, P.; Duez, P.; Dubois, J.; Ingrassia, L.; Lefranc, F.; Kiss, R.; Mijatovic, T. Balanitin-6 and -7:diosgenylsaponins isolated from Balanites aegyptiaca Del. display significant anti-tumor activity in vitro and in vivo. *Int J Oncol*, **2008**, *32*, 5-15.

LEGENDS TO THE FIGURES

Figure 1: *2i* **exerts cytostatic rather than cytotoxic effects on melanoma cells. A:** quantitative videomicroscopy illustrations of **2i**-induced effects on human SKMEL-28 melanoma cells after 72 h of treatment (5 μM). **B:** Videomicroscopic analysis was conducted twice in triplicate and quadruplicate, respectively. The global growth ratio was calculated, and data are presented as the mean ± SEM. **C:** Cell cycle analysis was performed on SKMEL-28 cells treated with 5 μM **2i** for 24, 48 and 72 h, respectively. **D:** Apoptosis measurement by TUNEL staining of SKMEL-28 cells treated for 24, 48 and 72 h with 5 μM **2i.** The manufacturer provided negative and positive controls (Ct − and Ct +, respectively), and we also used internal controls with PC-3 human prostate cancers cells left untreated or treated for 72 h with 1 μM narciclasine. The results are presented as the mean ± SEM (quadruplicate except for the kit controls, which are presented as the result in singulate).

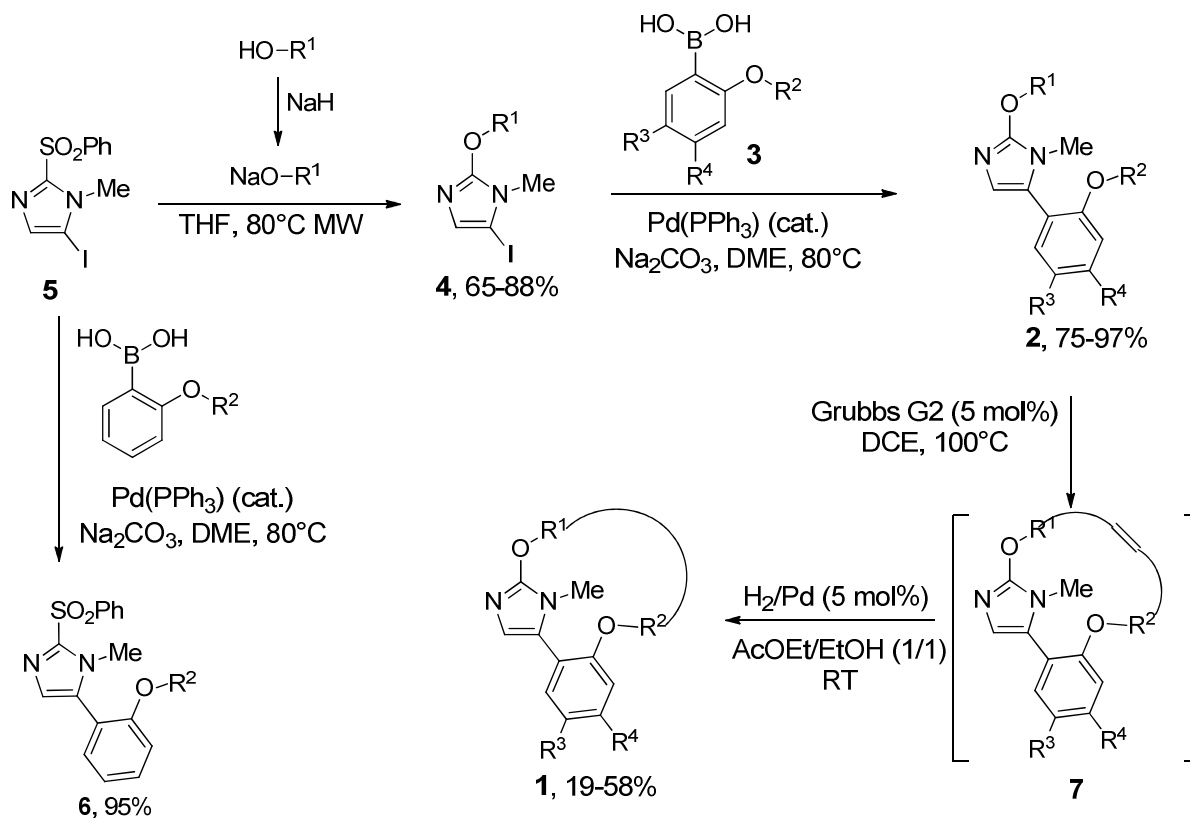**Figure 2: Characterization of the effects induced by 10 μM of *2i* in the NCI 60-cell-line panel.**

Figure 3: IC$_{50}$ values of *2i* compound on 11 human primary melanoma cultures. The dotted line corresponds to the mean IC$_{50}$ value obtained with these 11 primary cultures after **2i**-treatment for 72 h as revealed by the colorimetric MTT assay. Experiment was conducted once in sextuplicate. * indicates that the IC$_{50}$ is over 100 μM, i.e., the maximal concentration tested.

Figure 4: *2i*-**induced effects on mitochondria. A:** Mitochondrial staining with a fluorescent MitoTracker: fluorescence distribution and intensity was not altered by **2i** treatment over a 24 h period. **B:** ROS production over time was analyzed by flow cytometry in SKMEL-28 cells treated with 5 μM **2i**.

The results are presented as the mean ± SEM. **C:** Oxygen consumption analysis conducted after an

incubation of 72 h with 10 μM **2i** or left untreated (control). The results are presented as the mean ±

SEM of quadruplicates.

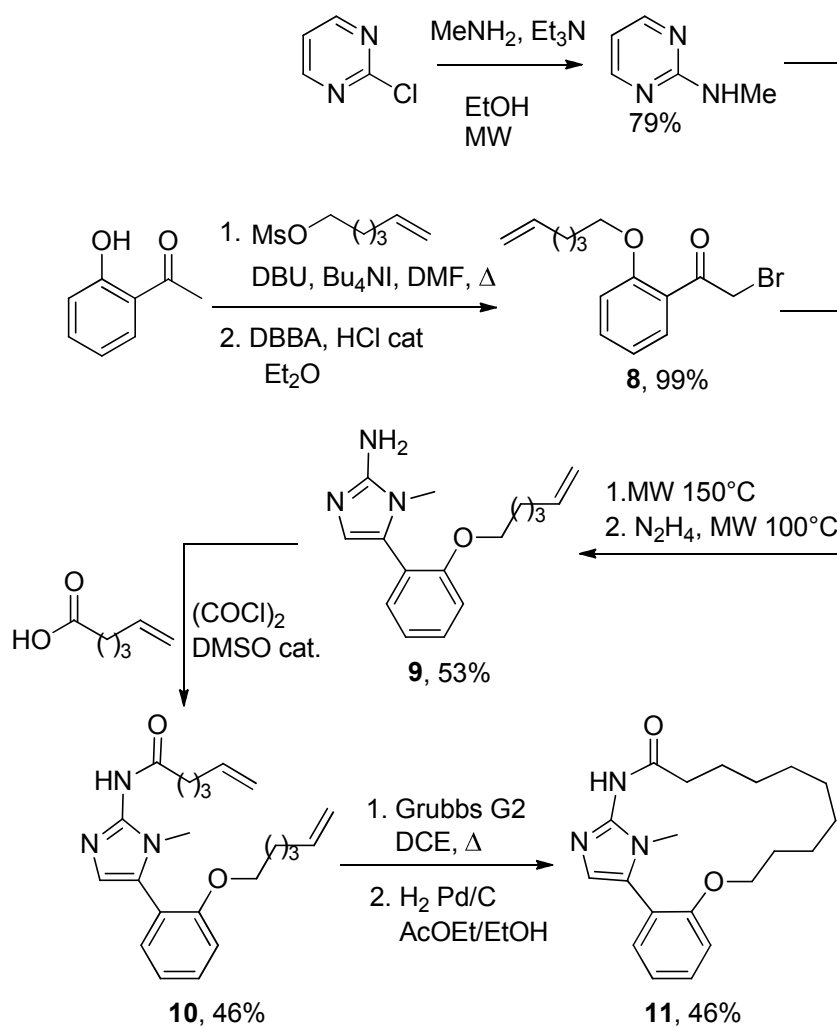**Figure 5.** Structure-activity relationship analysis and our lead compound **2i**.

1
2
3
Schemes and Tables
4
5
6
7
8
9
10
11
12
13
14
15
16
17
18
19
20
21
22
23
24
25
26
27
28
29
30
31
32
33
34
35

Scheme 1. Synthesis of 5-aryl-*1H*-imidazoles.

36
37
38
39
40
41
42
43
44
45
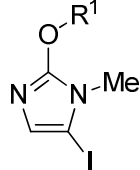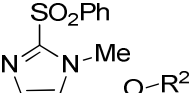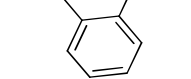46
47
48
49
50
51
52
53
54
55
56
57
58
59
60

Scheme 2. Synthesis of amide **11**.

Table 1. Compounds list and substituents with their mean IC$_{50}$ growth inhibitory concentrations determined by the colorimetric MTT assay after 72h incubation. Apoptosis sensitive cell lines (APO S) were PC3, MCF-7, LoVo and B16F10 while apoptosis resistant cell lines were U373, T98G, A549 and SKMEL-28. [§] B16F10 cells were not assayed. [*] U373 cells were not assayed.

Compound	Structure	R^1	R^2	R^3	R^4	R^5	IC50 (APO S)	IC50 (APO R)
(+/-)-1a[§]		(CH$_2$)$_8$		H	H	H	50 ± 1	68 ± 7
(+)-1a[§]		(CH$_2$)$_8$		H	H	H	43 ± 3	67 ± 3
(-)-1a[§]		(CH$_2$)$_8$		H	H	H	54 ± 6	71 ± 8
1b[§]		(CH$_2$)$_8$		Me	H	H	35 ± 1	54 ± 5
1c[§]		(CH$_2$)$_8$		OMe	H	H	35 ± 2	57 ± 6
1d[§]		(CH$_2$)$_8$		F	H	H	49 ± 3	70 ± 4
1e[§]		(CH$_2$)$_8$		H	F	H	38 ± 4	60 ± 6
1f[§]		(CH$_2$)$_8$		naphthyl		H	20 ± 3	26 ± 2
1g[§]		(CH$_2$)$_9$		H	H	H	55 ± 11	73 ± 2
1h[§]		(CH$_2$)$_{10}$		naphthyl		H	26 ± 1	26 ± 3
1i[§]		(CH$_2$)$_{10}$		H	H	H	29 ± 3	38 ± 4
1j[§]		(CH$_2$)$_{11}$		H	H	H	36 ± 3	47 ± 4
2a[§]		(CH$_2$)$_2$CH=CH$_2$	(CH$_2$)$_4$CH=CH$_2$	H	H	H	13 ± 3	22 ± 6
2b[§]		(CH$_2$)$_2$CH=CH$_2$	(CH$_2$)$_4$CH=CH$_2$	Me	H	H	51 ± 5	67 ± 14
2c[§]		(CH$_2$)$_2$CH=CH$_2$	(CH$_2$)$_4$CH=CH$_2$	OMe	H	H	38 ± 3	62 ± 7
2d[§]		(CH$_2$)$_2$CH=CH$_2$	(CH$_2$)$_4$CH=CH$_2$	F	H	H	44 ± 4	76 ± 6
2e[§]		(CH$_2$)$_2$CH=CH$_2$	(CH$_2$)$_4$CH=CH$_2$	H	F	H	56 ± 6	> 89 ± 6
2f[§]		(CH$_2$)$_2$CH=CH$_2$	(CH$_2$)$_4$CH=CH$_2$	naphthyl		H	21 ± 4	26 ± 2
2g[§]		(CH$_2$)$_3$CH=CH$_2$	(CH$_2$)$_4$CH=CH$_2$	H	H	H	13 ± 8	8 ± 4
2h[§]		(CH$_2$)$_4$CH=CH$_2$	(CH$_2$)$_4$CH=CH$_2$	naphthyl		H	33 ± 4	37 ± 9
2i		(CH$_2$)$_4$CH=CH$_2$	(CH$_2$)$_4$CH=CH$_2$	H	H	H	6 ± 1	7 ± 1
2j[§]		(CH$_2$)$_5$CH=CH$_2$	(CH$_2$)$_4$CH=CH$_2$	H	H	H	55 ± 12	70 ± 4

The structure (shown in the Structure column) bears substituents: O-R^1 and N-Me on an imidazole ring (N, N-Me), O-R^2, and R^3, R^4, R^5 on the aromatic ring.

1
2
3
4
5
6
7
8
9
10
11
12
13
14
15
16
17
18
19
20
21
22
23
24
25
26
27
28
29
30
31
32
33
34
35
36
37
38
39
40
41
42
43
44
45
46
47
48

Compound	Structure	R^1	R^2	R^3	R^4	R^5	IC50 (APO S)	IC50 (APO R)
2k*		C_4H_9	CH_3	H	H	H	59 ± 8	88 ± 4
2l*		C_6H_{13}	CH_3	H	H	H	31 ± 3	44 ± 6
2m*		$(CH_2)_4CCH$	CH_3	H	H	H	19 ± 6	30 ± 5
2n*		$CH_2(CF_2)_4CF_3$	CH_3	H	H	H	56 ± 7	77 ± 5
2o§		CH_3	CH_3	H	H	H	$> 91 \pm 9$	>100
2p§		$(CH_2)_2CH=CH_2$	CH_3	H	H	H	25 ± 1	25 ± 5
2q§		$(CH_2)_4CH=CH_2$	CH_3	H	H	H	11 ± 7	8 ± 2
2r*		$(CH_2)_4CH=CH_2$	CH_3	i-Pr	H	H	9 ± 3	4 ± 1
2s*		$(CH_2)_4CH=CH_2$	CH_3	Cl	H	H	29 ± 1	37 ± 6
2t*		$(CH_2)_4CH=CH_2$	CH_3	H	Cl	H	38 ± 2	55 ± 6
2u*		$(CH_2)_4CH=CH_2$	CH_3	H	H	OCH_3	26 ± 5	35 ± 5
2v*		$(CH_2)_4CH=CH_2$	CH_3	CF_3	H	H	57 ± 2	69 ± 10
2w*		$(CH_2)_4CH=CH_2$	CH_3	F	F	H	38 ± 2	45 ± 4
2x§		CH_3	$(CH_2)_4CH=CH_2$	H	H	H	77 ± 15	$> 91 \pm 5$
2y§		$(CH_2)_2OCH_2CH=CH_2$	$(CH_2)_4CH=CH_2$	H	H	H	31 ± 3	55 ± 7
2z*		$(CH_2)_3Ph$	CH_3	H	H	H	10 ± 6	3 ± 1
2aa§		$(CH_2)_4Ph$	CH_3	CH_3	H	H	33 ± 4	42 ± 1
(+/-)-7a*		$(CH_2)_2CH=CH(CH_2)_4$		H	H	H	59 ± 6	85 ± 5
4a§		$(CH_2)_4CH=CH_2$	/	/	/	/	$> 84 \pm 12$	> 100
6a§		/	H	H	H	H	$> 85 \pm 15$	> 100
6b§		/	$(CH_2)_4CH=CH_2$	H	H	H	28 ± 2	53 ± 9

Compound	Structure	R^1	R^2	R^3	R^4	R^5	IC50 (APO S)	IC50 (APO R)
6c[§]		/	$(CH_2)_2CH=CH_2$	H	H	H	47 ± 10	$> 83 \pm 10$
10[§]		$(CH_2)_3CH=CH_2$	$(CH_2)_4CH=CH_2$	H	H	H	14 ± 4	11 ± 4
11[§]		$(CH_2)_9$		H	H	H	52 ± 9	51 ± 6
14*		$(CH_2)_4CH=CH_2$	/	/	/	/	$>88 \pm 12$	>100
15*		$(CH_2)_4CH=CH_2$	CH_3	H	H	H	78 ± 4	$>97 \pm 3$

Table 2: Gene enrichment analysis of the genes detected as differentially expressed at their mRNA levels between the most sensitive and the most resistant melanoma primary cultures.

System	Gene Category	List Hits	List Total	Population Hits	Population Total	EASE score	Gene Symbol
Biological Process	energy pathways	16	206	189	9661	1.12E-05	ACADS; ACO2; ATP5B; COX17; COX6C; CS; FDXR; GAD1; HK1; IDH3A; MDH1; PPARD; PPP1R3C; S100B; SLC25A4; UQCRB
Cellular Component	mitochondrion	27	202	584	9551	2.23E-04	ACADS; ACO2; AMID; ATP5B; ATP6V1E1; C3ORF1; COX17; COX5B; COX6C; CPS1; CS; DECR1; FDXR; IDH3A; KIAA0196; MGST1; MLL; MRPS36; MTFMT; NDUFA5; NDUFA6; PHB; SIRT3; SLC25A16; SLC25A4; TOMM70A; UQCRB
Molecular Function	oxidoreductase activity	21	206	473	9859	1.98E-03	ACADS; AMID; BLVRB; COX5B; COX6C; DECR1; FADS2; FDXR; FLJ10661; FMO4; HSD17B12; IDH3A; MDH1; NDUFA5; NDUFA6; QDPR; RRM2B; SEPW1; TXN; UQCRB; VAT1
Cellular Component	inner membrane	9	202	120	9551	3.76E-03	ATP5B; ATP6V1E1; C3ORF1; COX5B; COX6C; KIAA0196; SLC25A16; SLC25A4; UQCRB

System	Gene Category	List Hits	List Total	Population Hits	Population Total	EASE score	Genes
Biological Process	energy derivation by oxidation of organic compounds	9	206	122	9661	4.38E-03	ACO2; CS; GAD1; HK1; IDH3A; MDH1; PPP1R3C; S100B; UQCRB
Cellular Component	mitochondrial membrane	10	202	152	9551	4.76E-03	AMID; ATP5B; ATP6V1E1; C3ORF1; COX5B; KIAA0196; PHB; SLC25A16; SLC25A4; UQCRB

System refers to the system of categorizing genes (e.g. "GO (gene ontology) Cellular Component") in the databases provided by the Ease software package. **Gene Category** refers to the specific category of genes within the System (e.g. "endoplasmic reticulum"). **List Hits** refers to the number of genes in the list of differential genes found in both genomic and transcriptomic comparisons that belong to the Gene Category. **List Total** refers to the number of genes of this list that belong to any Gene Category within the System. **Population Hits** is the number of genes in the total group of genes assayed (full list) that belong to the specific Gene Category. **Population Total** refers to the number of genes in the full list that belong to any Gene Category within the System. The **EASE score** is the probability value characterizing the change of proportion between the two ratios: population hits / population total and list hits/ list total. It constitutes the upper band of the distribution of leave-one-out Fisher exact probabilities computed on these two ratios.

Table of contents graphic

Cancer cell metabolism:
↑ O_2 consumption

2i

254x190mm (96 x 96 DPI)

1
2
3
4
5
6
7
8
9
10
11
12
13
14
15
16
17
18
19
20
21
22
23
24
25
26
27
28
29
30
31
32
33
34
35
36
37
38
39
40
41
42
43
44
45
46
47
48
49
50
51
52
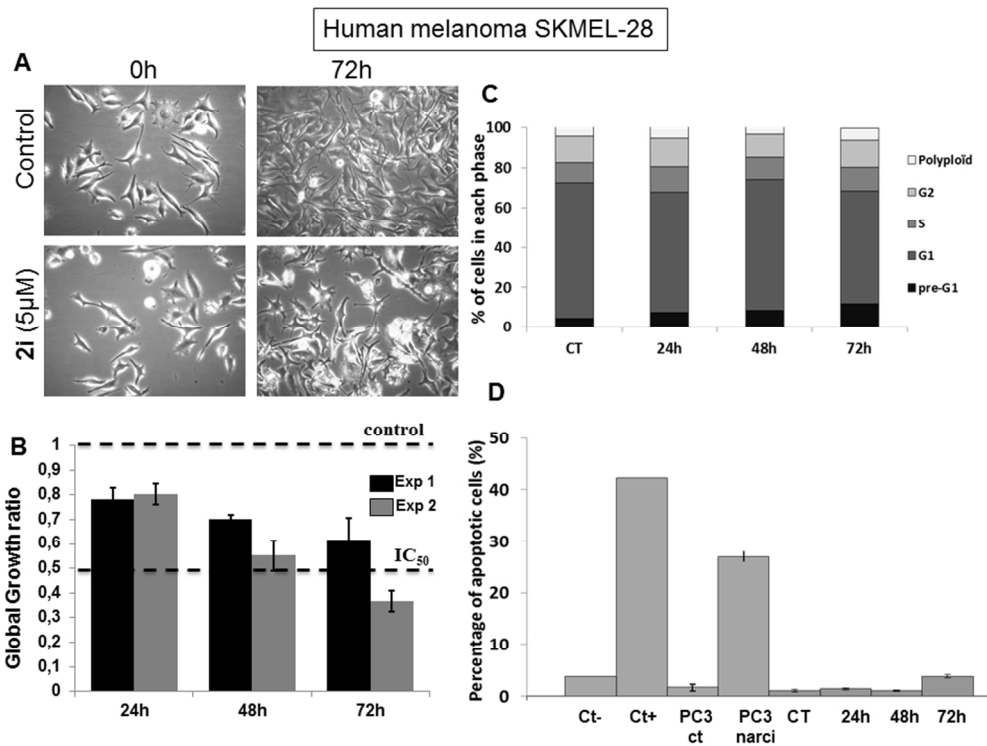53
54
55
56
57
58
59
60

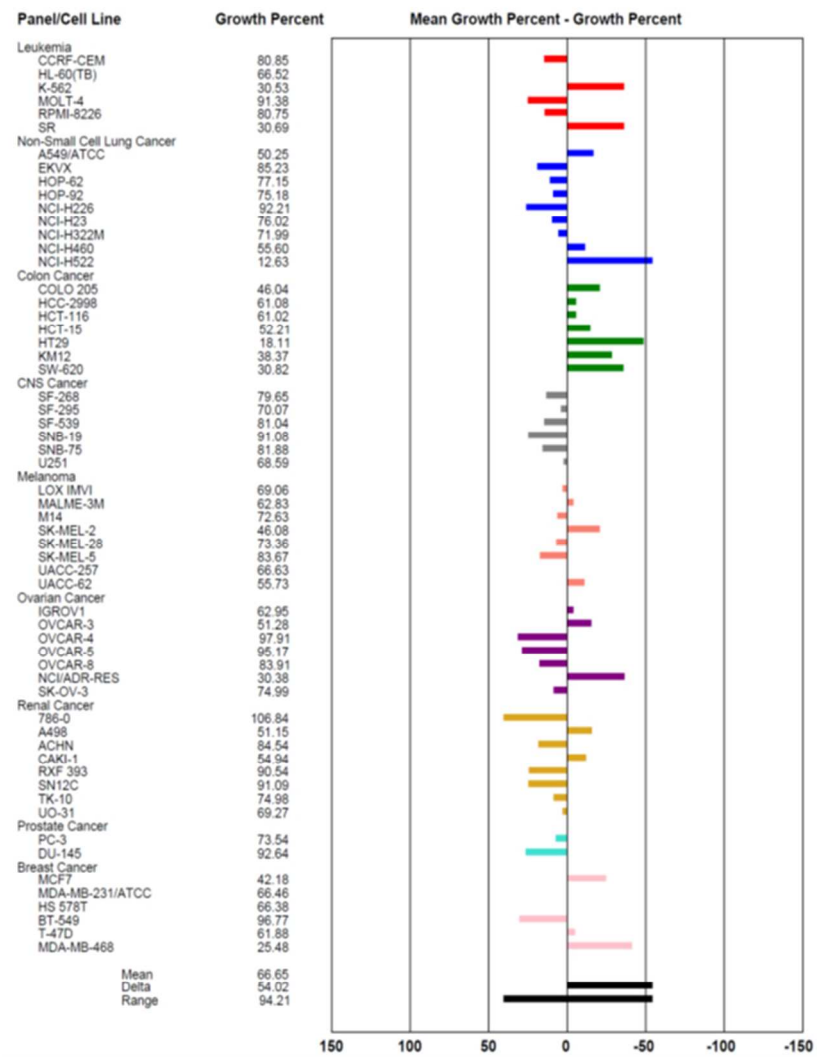| Panel/Cell Line	Growth Percent
Leukemia	
CCRF-CEM	80.85
HL-60(TB)	66.52
K-562	30.53
MOLT-4	91.38
RPMI-8226	80.75
SR	30.69
Non-Small Cell Lung Cancer	
A549/ATCC	50.25
EKVX	85.23
HOP-62	77.15
HOP-92	75.18
NCI-H226	92.21
NCI-H23	76.02
NCI-H322M	71.99
NCI-H460	55.60
NCI-H522	12.63
Colon Cancer	
COLO 205	46.04
HCC-2998	61.08
HCT-116	61.02
HCT-15	52.21
HT29	18.11
KM12	38.37
SW-620	30.82
CNS Cancer	
SF-268	79.65
SF-295	70.07
SF-539	81.04
SNB-19	91.08
SNB-75	81.88
U251	68.59
Melanoma	
LOX IMVI	69.06
MALME-3M	62.83
M14	72.63
SK-MEL-2	46.08
SK-MEL-28	73.36
SK-MEL-5	83.67
UACC-257	66.63
UACC-62	55.73
Ovarian Cancer	
IGROV1	62.95
OVCAR-3	51.28
OVCAR-4	97.91
OVCAR-5	95.17
OVCAR-8	83.91
NCI/ADR-RES	30.38
SK-OV-3	74.99
Renal Cancer	
786-0	106.84
A498	51.15
ACHN	84.54
CAKI-1	54.94
RXF 393	90.54
SN12C	91.09
TK-10	74.98
UO-31	69.27
Prostate Cancer	
PC-3	73.54
DU-145	92.64
Breast Cancer	
MCF7	42.18
MDA-MB-231/ATCC	66.46
HS 578T	66.38
BT-549	96.77
T-47D	61.88
MDA-MB-468	25.48
Mean	66.65
Delta	54.02
Range	94.21

190x254mm (96 x 96 DPI)

1
2
3
4
5
6
7
8
9
10
11
12
13
14
15
16
17
18
19
20
21
22
23
24
25
26
27
28
29
30
31
32
33
34
35
36
37
38
39
40
41
42
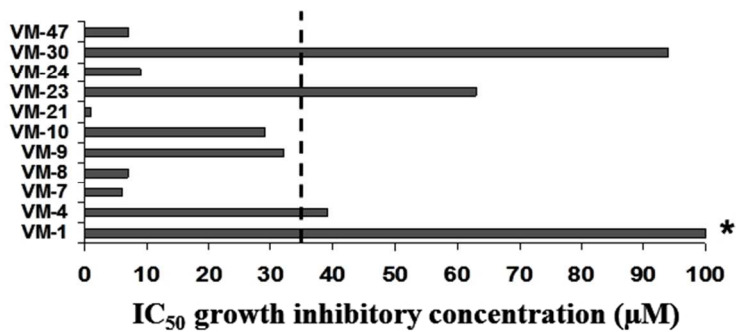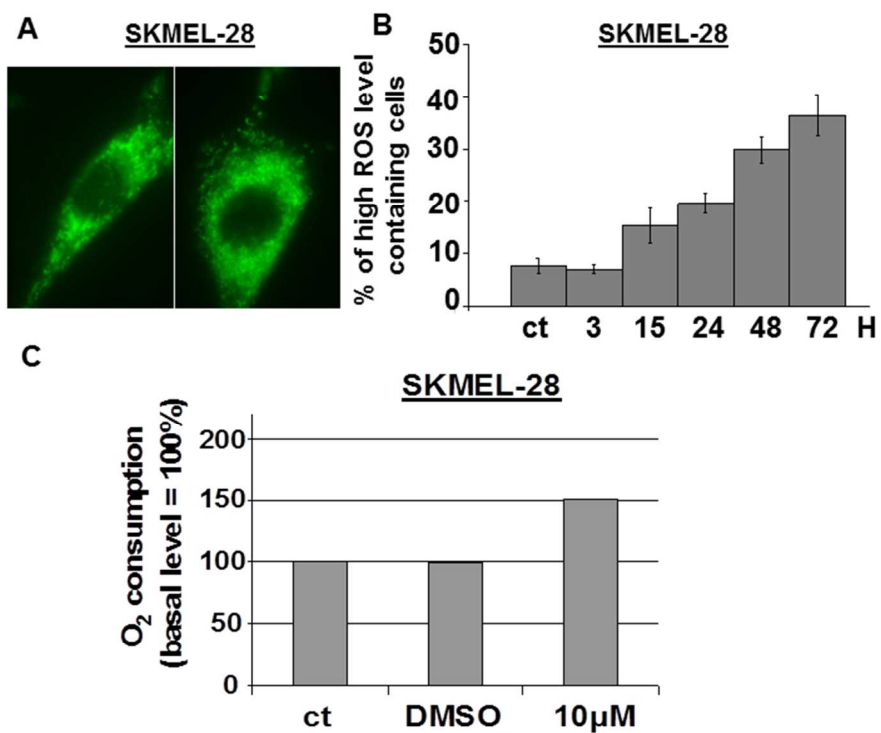43
44
45
46
47
48
49
50
51
52
53
54
55
56
57
58
59
60

190x254mm (96 x 96 DPI)

1
2
3
4
5
6
7
8
9
10
11
12
13
14
15
16
17
18
19
20
21
22
23
24
25
26
27
28
29
30
31
32
33
34
35
36
37
38
39
40
41
42
43
44
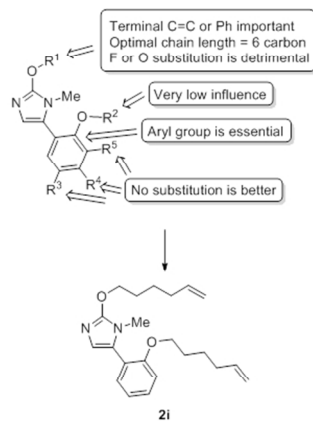45
46
47
48
49
50
51
52
53
54
55
56
57
58
59
60

190x254mm (96 x 96 DPI)

1
2
3
4
5
6
7
8
9
10
11
12
13
14
15
16
17
18
19
20
21
22
23
24
25
26
27
28
29
30
31
32
33
34
35
36
37
38
39
40
41
42
43
44
45
46
47
48
49
50
51
52
53
54
55
56
57
58
59
60

254x190mm (96 x 96 DPI)